CO-AGGREGATION STUDIES OF NUCLEIC ACID NANOSTRUCTURES WITH TETRACYCLINE MOLCULES

By

NOUF ALZAHRANI

A thesis submitted to the

Graduate School-Camden

Rutgers, The State University of New Jersey

In partial fulfillment of the requirements

For the degree of Master of Science

Graduate Program in Chemistry

Written under the direction of

Jinglin Fu

And approved by

_____

Jinglin Fu, Ph.D.

_____

David Salas-de la Cruz, Ph.D.

_____

Hao Zhu, Ph.D.

Camden, New Jersey

May 2018

THESIS ABSTRACT

Co-aggregation Studies of Nucleic Acid Nanostructures with Tetracycline Molecules

By

NOUF ALZAHRANI

Thesis Director:

Jinglin Fu, Ph.D.

Biological systems have evolved complex macromolecular nanostructures to carry out cellular functions with high specificity and efficiency, such as mitochondrial electron-transport chains, polymerase and transcription cofactors and light-harvesting antenna in photosynthesis. These organized nanostructures are formed inside cells by spontaneous self-assembly of individual molecular components. In the past few decades, researchers have taken advantage of the self-assembly of nucleic acids to construct various 1D – 3D nanostructures. Self-assembled DNA nanostructures have an inherent advantage of generating programmable nanostructures with controllable parameters of dimension, structural hierarchy and nanometer precision, which can be used for mediating drug release. In this thesis, we have studied single- or double-stranded DNA molecules for forming nanoparticles with minocycline (MH) in the presence of magnesium ions (bridging effect) and π-π stacking interaction. We evaluated multi-dimensional DNA nanostructures (e.g. ssDNA, dsDNA, DNA origami) to load and release MH with sufficient dose during an interval of two weeks. The entrapment efficiency of MH and DNA was found to depend on the Mg^{2+} concentration, DNA length, and types of DNA (i.e. as a function of nitrogen

bases). The molecule ssDNA with length > 11-nucleotide (nt) was found to form aggregates with MH in the presence of Mg^{2+}. The titration of Mg^{2+} concentration showed that the maximum particle formation yield was reached at ~ 4 mM. ssDNA also showed higher dimensional aggregate formation yield than dsDNA, due to the flexible structure of ssDNA allowing more aggregation with MH and Mg^{2+}. In collaboration with Drexel University, we have applied DNA-Mg^{2+}-MH particles to agarose gel encapsulation and release for maintaining the activity of MH during a long-period release. This DNA-mediated MH release could be potentially used in the future spinal cord therapy for localized delivery of MH at the injury site.

Dedication

I dedicate this dissertation to my beloved husband, parents, and sons. Without them, this dissertation would have never been written. I am grateful to have them in my life.

Acknowledgments

I am deeply thankful to my lovely family for making success possible and rewarding. My special thanks go to my dear husband Abdullah Almalki who encouraged me to reach my dreams, and motivated me when I needed it the most. I am thankful to my parents Matoq, and Norah for their constant love and endless support. To my grandparents for their prayers and words of wisdom. To my caring brothers (Abdullah & Abdulrahman) and sister (Sarah) for their continuous encouragement. To my beautiful little Mohanned and Mourad who have been my motivation, inspiration and drive.

I am thankful to my advisor Dr. Jinglin Fu for his guidance and support. I am also grateful to Dr. David Salas-de la Cruz, and Dr. Hao Zhu for serving in my committee and for their time and advise.

Finally, I am thankful to my country for their scholarship, and funding my education.

Table of Contents

List of figures

Chapter 1

Introduction

Abstract

Deoxyribonucleic acid (DNA) is a self-assembled biopolymer that carries genetic information. Recent breakthroughs in DNA origami and single-stranded DNA bricks have empowered the design and fabrication of a virtually unlimited reservoir of spatially addressable 1D, 2D and 3D nanostructures, including structures with complex curvatures, polyhedral meshes and periodic DNA crystals. DNA scaffold-directed assembly holds great promise to organize bioactive therapeutics with precise control of spatial patterning. These DNA structures are used as assembly platforms to organize various elements and particles on nanoscale and produce new functional materials. DNA nanotechnology is being applied to different fields, including biomaterials, photonics, nanotechnology, and nanomedicine.

1.1. Structural DNA Nanotechnology.

Biological systems utilize complex macromolecular nanostructure networks that have specificity and high efficiency to mediate cellular functions, such as bimolecular synthesis, gene expression, regulation, and signal transduction. The structures of these networks are the result of self-assembly of the molecules into highly organized spatial structures, where the determination of the relative position of molecules is precisely controlled to facilitate functionality. For example, these components must be specifically structured to enable functions, such as biochemical synthesis and photosynthesis. In recent decades, researchers have taken advantage of the self-assembly processes of molecules in

peptides, nucleic acids, lipids, and polysaccharides to construct different types of nanostructures, including nanofibers, vesicles, and nanotubes. Nevertheless, accurate arrangement of multiple heterogeneous components with nanometer precision and geometric manner is still a challenge. DNA is more promising than some biomolecules for the construction of complex bimolecular networks. DNA is a self-assembled biopolymer that consists of nucleotides that contain deoxyribose sugar, a phosphate backbone, and a nitrogen base. These nucleotides are stabilized by stacking interactions (π-π stacking), hydrogen-bonding, and hydrophobic interactions [1]DNA is generally defined as a hereditary molecule that stores biological information as code and transfers it from generation to generation. Moreover, it is a well-defined structural nanomaterial. In B-form DNA double helices, the distance between two bases is 0.34 nm ($3.4A^0$), helical repeat is ~3.4nm, and diameter is 2 nm, as shown in **Figure 1.** [1 , 2]

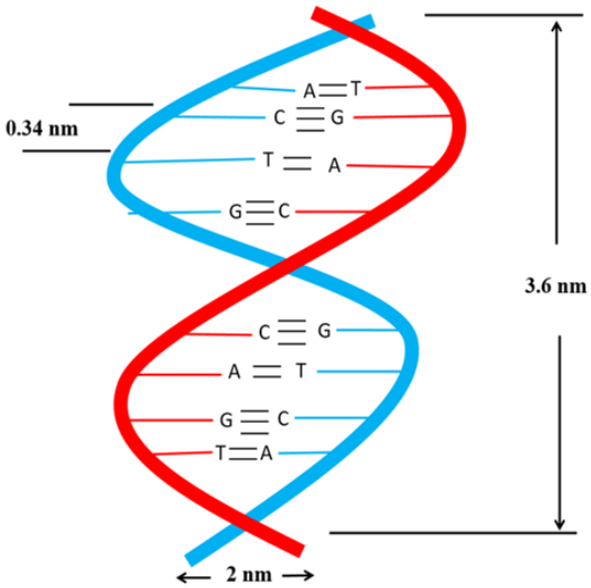

Figure 1. Double helical dsDNA schematic representation. (This figure is reconstructed from another publication) [3]

DNA is a "bottom-up" construction in nanotechnology that can be used for building nanoscale materials.[2] DNA was discovered in the 1970s, when short single strand was sticking out from the end of a complementary double-stranded DND and joined another DNA, forming different DNA assembly nanostructures with controlled intermolecular interactions and programmable systems.[1-2] As **Figure 2** illustrates, unique number structures of DNA nanotechnology has been constructed, including multi-helix bundles and nanotubes, (**Figure 2A**), 2D lattice arrays and squares (**Figure 2B**), and 3D geometric shapes, such as cubes, tetrahedrons, and buckyballs. (**Figure 2C**). [1]

Figure 2. Examples of structural DNA nanotechnology: (A) DNA helix bundle, (B) 2D arrays, (C) 3D shapes. [1]

In addition, aperiodic structures in DNA nanotechnology have been created by using DNA strands as scaffolding.[4] DNA scaffold strands, such as M13 bacteriophage DNA, can anneal with short DNA (staple strands) as shown in **Figure 3A**, forming 2D DNA origami (**Figure 3B**). Multilayer DNA origami can form nanotubes, which are 3D DNA origami, as shown in **Figure 3C**.[5]

Figure 3. DNA origami structures: (A) the scaffold strands of DNA, [6] (B) 2D origami, [6] (C) 3D origami. [4]

Single-stranded DNA tile (SST) assembly is another type of three-dimensional DNA architecture. They are based on single strand tiles that have 32 nucleotides with four domains, as shown in **Figure 4A**. The binding domains are flexible, allowing the strands to assemble with each other to form a Lego-like model. Each two bricks have two complementary 8nt domains (**Figure 4B**), or a 3D canvas of DNA (**Figure 4C**). [7 8]

Figure 4. Schematic of DNA bricks: (A) Domains of single strand tile, [7](B) Assembly of two domains to forming Lego model, [7](C) 3D canvas. [8]

1.2. DNA-Based Drug-Delivery Vehicles and Advanced Therapeutics.

Many prototypes of DNA-nanotechnology have been applied to drug delivery and therapeutics in pharmacology.[9] For example, self-assembled DNA nanostructures are used to control cancer cell progression.[10 5] Anti-cancer drugs, such as Doxorubicin, can be incorporated into double-stranded DNA structures for delivering into cancer cells to induce

apoptosis for killing cancer cells.[10] DNA nanostructures also demonstrated potentials for the ttreatment of metabolic diseases, infections, inflammation, and autoimmune diseases.[10] The properties of DNA including self-assembly and nanoscale size can be used to develop innovated programmable shapes with high efficiency for cellular delivery for different uses. As shown in **Figure 5A and 5B**, DNA origamis were assembled into the shape of a tetrahedron or box with lid to deliver payloads and control their release to targeted cells. [10] Triangle-shaped DNA origami and twisted 3D rods were used to carry anti-cancer drugs (**Figure 5C)**. [5]

Figure 5. (A & B)Nanobox made by DNA origami, [10] (C) 3D DNA origami. [5]

Further, self-assembled DNA tetrahedron has demonstrated the ability to deliver small interfering RNA (siRNA) into targeted tumor cells by using ligands such as folate or peptides (as shown in **Figure 6A**). [11] [12] Recently, DNA origami tube nanostructures have been used as potential noncytotoxic immunostimulants to carry cytosine-phosphate-guanine (CpG) sequences. By the endocytosis process, the DNA origami tube carrying CpG sequences enters the cell and is recognized by the Toll-like receptor 9 (TLR9), a specialized receptor of the immune system. Hence, DNA origami carrying CpG sequences induces cellular immunostimulation and secretes cytokine, which is a small protein that is responsible for cell signaling. Studies have shown that production of cytokine induced by

DNA origami tube decreased in the absence of CpG (see **Figure 6B**). [12] DNA aptamer has also been successful in DNA nanostructure-based drug delivery, due to its high specificity and affinity for anti-cancer drug. [13] It enhances recognition of the drug by the cancer cell and reduces side effects (see **Figure 6C**). [12]

Figure 6. Examples of DNA-based drug delivery vehicles: (A) DNA tetrahedron with siRNA, (B) intracellular delivery of immunostimulatory CpG oligonucleotides, (C) loading Dox by using aptamer.[12] [14]

1.3. DNA binding with small-molecule analogues.

Recently, DNA nanostructures have been studied to bind with a wind range of small molecule analogues and drugs. DNA has several advantages for binding to small molecules, including its nanoscale size of 1-100 nm, biocompatible components, highly programmable and controllable structures and improved stability under intracellular environment.[12] Thus, DNA has suitable properties for serving as drug delivery systems. It assembles with one or more drugs to enhance their delivery to targeted cells without affecting the capability or effectiveness of the drugs, decreases their toxicity, and enables their transcellular transport across the epithelial and endothelial barriers and the cell

membrane.[12,15] DNA structures are negatively charged and in some applications, it can bind with cationic polymers.[16,17] As shown in **Figure** 7, cationic polymer binds with DNA through electrostatic interaction on phosphate groups, forming colloidal aggregates called polyplexes.[18]

Figure 7. Schematic illustration of polyplexes. [16]

1.3.1. Cyanuric Acid (CA):

Several published studies have demonstrated that DNA binds with small molecules to enhance their release or activity. Cyanuric acid (CA) includes three thymine-like faces and induces the reprogramming of the assembly of unmodified DNA (poly adenine, or Poly(A)) as shown in **Figure 8**. Poly(A) interacts with thymine through hydrogen bond and forming duplex or triplex structures, which has prospective applications in drug delivery due to the formation of biocompatible components. [19]

Figure 8. Illustration of CA-adenine complementary hybridization with three thymine-like faces. [19]

1.3.2. Doxorubicin (DOX):

Doxorubicin (DOX) is an anticancer drug which has been used for several types of cancers including breast, thyroid, and ovarian. However, it has numerous side effects, poor selectivity, and cardiotoxicity. [12 20] Recent studies have shown that carriers such as gold nanoparticles (AuNP), polymers, and liposomes can assist to deliver the drug with high efficiency and reduced toxicity. Using AuNP, the double helix of DNA can intercalate the DOX to release it into the targeted cell. **Figure 9A** illustrates the process of drug loading and release. [21] DNA origami has been used to deliver DOX to targeted human cancer cells with high effectiveness against the cancer cells [22 23] A DNA origami delivery system was designed for three types of breast cancer cell lines (MDA-MB-231, MDA-MB-468, and MCF-7) with different degrees of global twist (see **Figure 9B**). The different degrees of global twist cause relaxation in the DNA double-helix structure when DOX intercalates to the DNA. Consequently, the encapsulation yield of the DOX is tunable, cytotoxicity is increased, and intercellular elimination is decreased compared to free DOX. [12 23]

Figure 9. (A) Schematic illustration of loading and release of DOX [21], (B) DNA origami delivery system for cancer therapy with tunable release. [23]

1.4. Conclusion.

In summary, DNA has recently emerged as an extremely promising biomaterial to organize molecules on the nanoscale. Super-molecular networks of molecules that are scaffolded by DNA nanostructures exhibit well-controlled inter-component distances and relative molecular ratios. Self-assembled DNA nanostructures thus serve as delivery platforms that are integrated with various functions ranging from molecular recognition and computations, dynamically structural switch to carrying molecular payloads and selectively release. Single- or double-stranded DNA (ssDNA or dsDNA) molecules can also bind to small drug molecules, such as doxorubicin, daunorubicin and epirubicin. In this thesis, we discovered that DNA was able to bind with MH molecules and form nanoparticles.

Chapter 2

Investigation of DNA- Mg^{2+}-MH Particles Formation

Abstract

In this chapter, we investigated how minocycline hydrochloride (MH) co-aggregated with DNA molecules and form particles precipitation. Mg^{2+} was proposed to work as "bridging molecules" to crosslink DNA with MH. Several factors were studied to affect DNA- Mg^{2+}-MH co-aggregation, including divalent metal ion (Mg^{2+}), DNA length, and DNA different nitrogen bases. MH also discriminated between ssDNA and dsDNA in which MH-ssDNA complex was high entrapment yield than MH-dsDNA complex.

2.1. Minocycline Hydrochloride (MH).

Minocycline hydrochloride (MH) is a zwitterionic compound that is part of the semi-synthetic tetracycline family. [24]It works as an anti-apoptotic, anti-inflammatory, and anti-oxidative as well as against both gram-positive and gram-negative bacteria. Particularly worth noting are its high absorption and good tissue penetration characteristics which have made it useful to cure a variety of diseases. MH has been shown to prevent smooth muscle cell reproduction, migration, and neointima formation after arterial injury by prohibiting expression of certain matrix metalloproteinases.[25] MH also protects cardiac myocytes against ischemia reperfusion injury, reduces inflammation, and protects against brain ischemia.[26] It has been used to treat spinal cord injury, benign and malignant tumors,[27] Alzheimer's disease,[12] multiple sclerosis,[28] Huntington's disease [29], and Parkinson's disease. [30]

Based on human studies, the standard dose of MH is 3 mg/kg. To cure diseases, high doses are required over a long period of time.[31 32] However, high concentrations of MH have led to side effects such as liver toxicity and death in experimental animals.[33] For instance, previous studies have investigated the use of MH in inhibiting smooth muscle cell reproduction, migration, and neointima formation after arterial injury by prohibiting expression of certain matrix metalloproteinases, 70-100 mg/kg doses of MH were used to reduce neointima formation in rats.[25] In studies on Parkinson's disease, 120 mg/kg doses of MH were found to protect dopamine neurons against 1-methyl-4-phenyl-1,2,3,6-tetrahydropyridine (MPTP).[30] Previous studies have illustrated that, to retain the efficiency of MH, a drug delivery system was used to deliver the drug to the target position because it has high water solubility and rapidly diffuses to an aqueous environment.[32] When combined with a neuroprotective agent (methylprednisolone) in the presence of hydrophobic poly lactic-co-glycolic acid (PLGA) to control the rate of release, MH displayed high loading efficiency in the treatment of spinal cord injury.[32 33]

Tetracyclines were discovered in 1948 as products of the natural fermentation of Streptomyces aureofaciens, a soil bacterium.[34] There are three current analogues for tetracycline: natural tetracycline products, semi-synthetic tetracycline compounds, and chemically modified tetracyclines.[35] MH is a tetracycline analogue that has four rings that are similar to tetracycline except that the diethylamino group is substituted at C7 and a functional group is lacking at C6 (as shown in **Figure 10**) making the drug more distributive into tissue and organs.[36 37] MH chelates with divalent metal ions, such as Ca^{2+} or Mg^{2+}, forming an insoluble complex with a positively charged molecule, that can been interacted with a negatively charged molecule, such as dextran sulfate (DS). [38]

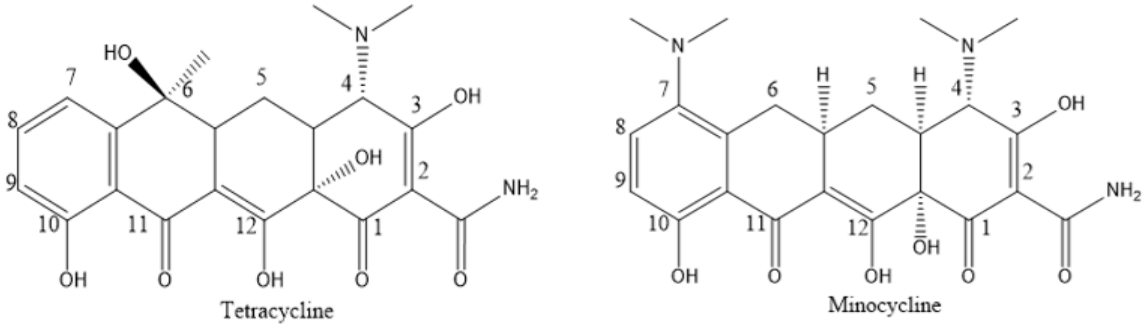

Figure 10. Chemical structures of tetracycline and minocycline.

2.2. Hypothesis of DNA-Mg^{2+}-MH complex.

Minocycline hydrochloride (MH) is proposed to interact with DNA through electrostatic interaction, Mg^{2+} bridge, and pi-pi stacking. MH is zwitterionic molecule that has four pKa values, 2.8 and 7.8 for the two hydroxyl groups at C3 and C10, respectively, and 5 and 9.5 for the two amine functional groups on C7 and C4, respectively, as shown in **Figure 11B**. Thus, it has both positive and negative charged groups. Through electrostatic interaction, deprotonation of the hydroxyl group at C3 will occur with one negatively charged on C3 and one positively charged on C4 at ammonium group. With positively charged on C4, the DNA molecule could bind with MH through phosphate group. Hydroxyl group on DNA may also potentially form hydrogen bonding with carbonyl, hydroxyl, and amide groups in MH. Furthermore, DNA's aromatic bases can interact with MH's aromatic rings through pi-pi stacking. To increase the aggregation of DNA-MH particles, Mg^{2+} can work as "bridge agents" to crosslink DNA with MH, as well as enhance the electrostatic interaction between multiple DNA-MH strands. In the bridging, the negatively charged of phosphate group of DNA bind with negatively charged of hydroxyl group in MH via Mg^{2+} bridge and forming insoluble particles, as illustrated in **Figure 11C**.

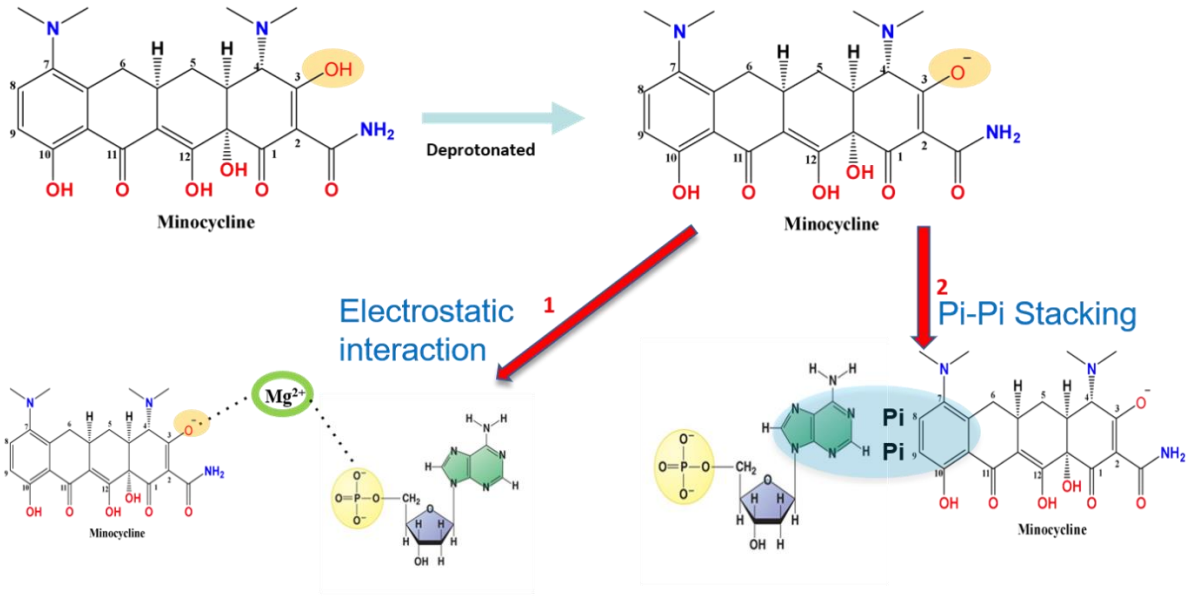

Figure 11. Cartoon representation of chemical structure of: (A) DNA, (B) minocycline hydrochloride, (C) complex formation of MH-Mg^{2+}-DNA.

The innovation of this study is to develop a novel drug carrier/delivery system capable of modulating the loading and release kinetics of drug molecules. As a carrier system, self-assembled DNA nanostructures have an inherent advantage of generating programmable nanostructures with controllable parameters of dimension, structural hierarchy and nanometer precision. Compared with conventional polymer-based drug delivery, the DNA-scaffold based drug delivery offers the following features: 1) the ability to modulate multiple interactions between DNA and organic drug molecules including electrostatic metal ion bridging and pi-pi stacking; 2) the feasibility to easily tune the dimensional parameters of the molecular scaffold to carry drug molecules; 3) the control over the drug release kinetics by the rationally designed surface-to-volume ratio and drug diffusion through the multi-layer nanostructures; 4) the possibility of switching the release

kinetics via the structural transformation of DNA nanostructures; 5) the ability to offering an ideal drug release paradigm for spinal cord therapy. In addition to MH, DNA nanostructures can potentially be used to load and release proteins and peptides and small molecule drugs such doxorubicin, daunorubicin and epirubicin. Therefore, this study not only leads to the development of an effective treatment for MH, but also has great potential to generate a variety of drug delivery systems for various biomedical applications in the future.

2.3. Materials and methods.

2.3.1. Materials

Tris base and acetic acid buffer (10 × TA) were purchased from Fisher Scientific (Waltham, MA.) and Mallinckrodt, respectively. DNA grade water and Magnesium acetate tetrahydrate (MgAc) were purchased from Fisher Scientific (Waltham, MA.). Oligonucleotides were synthesized and purchased from Integrated DNA Technologies (IDT). Minocycline hydrochloride was purchased from Sigma (St. Louis, MO.).

2.3.2. Preparation of MH-metal ion-DNA complex.

A) Preparation of MH- metal ion as control.

To observe what may happen and compare when the independent variable was changed, using a control in an experiment is required. In this study, the control is minocycline solution, which was prepared in DNA grade water with final mass concentration(1mg/ml), followed by the addition of different concentrations of magnesium acetate (0, 1, 2, 4, 8, 16 mM), 1 X TA buffer (pH 7.0), and deionized water (DI). The complex solution was vortexed and then incubated in the dark for 30 minutes on a rocker (ARMA/Rock 100 Shaker) under room temperature (~ 25 °C) at 50 rpm, followed by

centrifugation at 10,000 rpm for 10 min at 4 ˚C. The controls were loaded in the wells of the UV-96-well half area plate. The loading efficiency of minocycline with the metal ion was measured by monitoring the absorbance at 350nm.

B) Preparation of MH-metal ion-DNA complex.

DNA oligonucleotides were dissolved in DNA grade water. Solution's concentration was measured by Nanodrop 2000 (Thermo Scientific). Minocycline solution was prepared in DNA grade water. DNA-MH solution was mixed with equal mass concentration (1mg/ml) followed by the addition of different concentration of magnesium acetate (0, 1, 2, 4, 8, 16mM),1 X TA buffer (PH 7.0), and deionized water (DI). The complex solution was vortexed to induce complex formation and then incubated in the dark for 30 minutes on a rocker (ARMA/Rock 100 Shaker) under room temperature at 50 rpm, followed by centrifugation at 10,000 rpm for 10 min at 4^0C. The supernatant of the samples was loaded in the wells of the UV-96-well half area plate < 300 nm. The loading efficiency of minocycline with DNA was measured by monitoring the absorbance at 350nm and 260nm for MH and DNA, respectively. Entrapment efficiency and loading efficiency of the MH-metal ion-DNA complex were determined by the **following equation:**

Encapsulation yield of DNA=

$$\frac{\text{Absorbance value of DNA at 0mM } Mg^{2+} \; - \; \text{Absorbance value of DNA at } \mathbf{x} \text{ mM } Mg^{2+}}{\text{Absorbance value of DNA at 0mM } Mg^{2+}}$$

Where X= 0, 1, 2, 4, 8, 16 mM Mg^{2+}

Encapsulation yield of MH=

$$\frac{\text{Absorbance value of MH in control} - \text{Absorbance value of MH in sample}}{\text{Absorbance value of MH in control}}$$

Molar ration of MH to nucleotide= $\frac{\text{Molar ratio of MH to DNA}}{\text{Monomer number of DNA}}$

2.4. Results and Discussion.

2.4.1. Investigation of magnesium concentration on the formation of MH-DNA particles.

To evaluate the Mg^{2+} bridging effect, we first tested the formation of DNA-Mg^{2+}-MH particles depending on Mg^{2+} concentration. As shown in **Figure 12**, two set of samples were prepared: A control solution containing MH and Mg^{2+}; and a sample solution containing poly(A)20, MH and Mg^{2+}. In **Figure 12A**, for control solution, there is no observed formation of MH particles with the addition of Mg^{2+} from 0 to 16 mM. As shown in **Figure 12B**, no particle formation was observed for DNA and MH without the addition of Mg^{2+}. However, as the addition of Mg^{2+}, it was observed the formation of yellow particles of DNA- Mg^{2+}-MH complex. To quantitatively analyze the formation of particles, the absorbance spectrum of supernatant solution of DNA-Mg^{2+}-MH complex were characterized from 220 nm to 450 nm (**Figure 12C**). The absorbance of MH-PolyA(20) solution was decreased as increasing Mg^{2+} concentration, which indicated that there was particle formation as the increase of Mg^{2+} concentration.

To validate the bridging effect of divalent Mg^{2+}, we performed a NaCl competition assay for the formation of DNA- Mg^{2+}-MH particles. Na^{+} is a monovalent ion, and it can

disrupt the electrostatic Mg^{2+} bridging by saturating DNA backbone phosphate and MH molecules. As shown in **Figure 13**, the formation yield of DNA- Mg^{2+}-MH particles decreased dramatically as the addition of Na^{+} from 0 to 1000 mM, and the particles were completely disappeared at 1000 mM Na^{+} (performed by Dong Gyu Yang). This result demonstrated that DNA-MH particles were stabilized by Mg^{2+} bridging effect, and were disrupted by monovalent ion competitor.

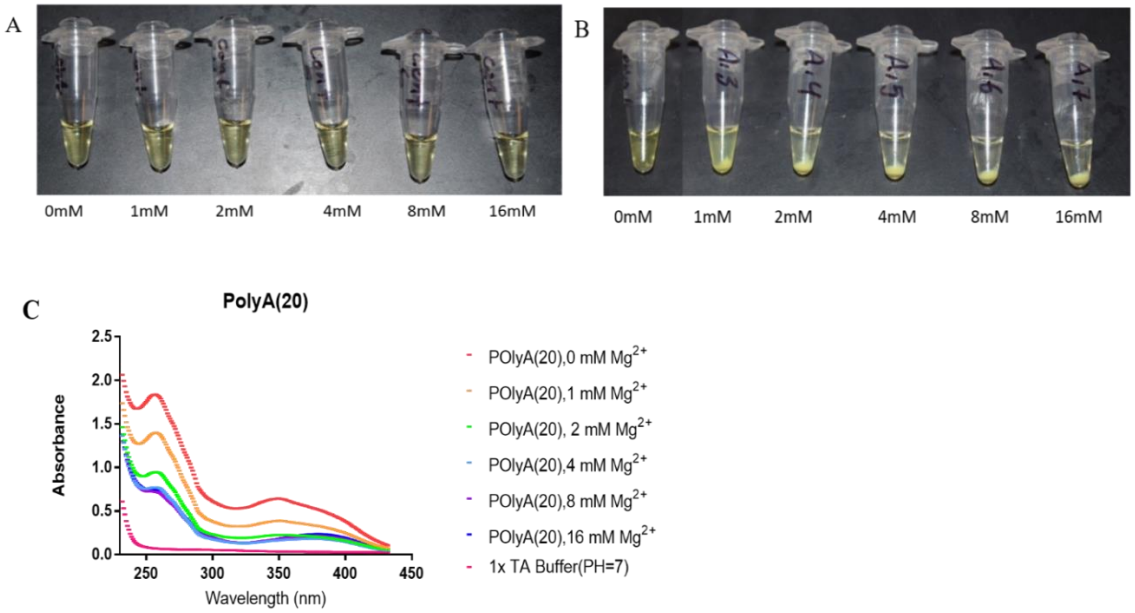

Figure 12. Observation of the metal ion-mediated complex with different concentrations. (A): Controls solution of MH and Mg^{2+}, (B) Sample solutions composed of DNA (Poly(A)20) with MH and Mg^{2+} mediated the complex, (C) Absorbance data of Poly(A)20.

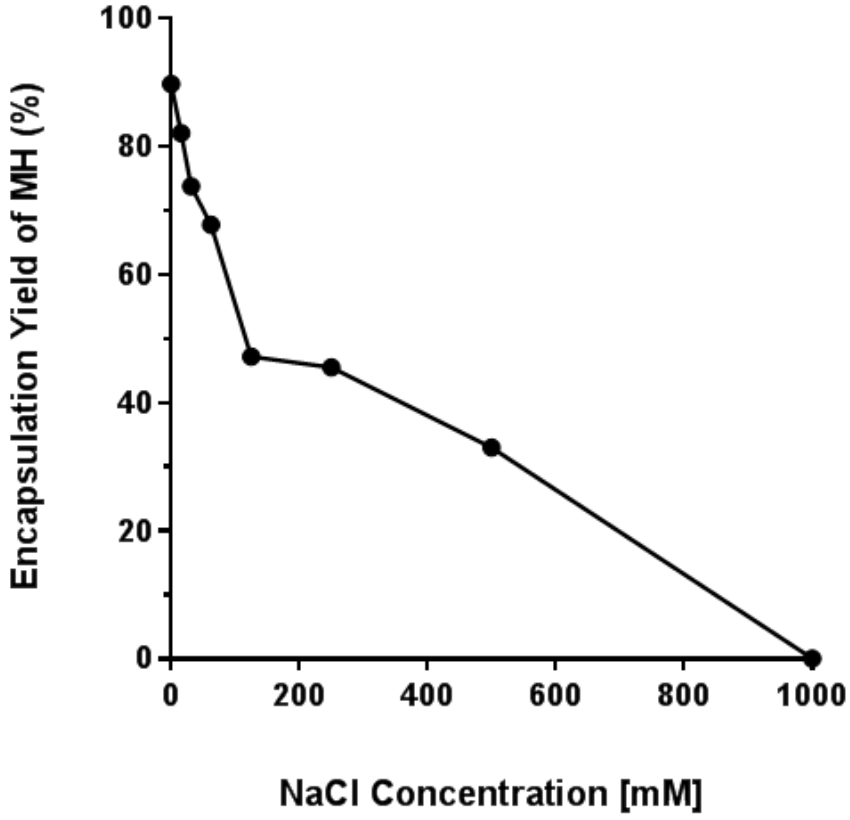

Figure 13. NaCl competition assay for the formation of DNA-Mg2+-MH particles. NaCl is added into a mixture of poly(A)20- Mg^{2+} (4 mM)-MH.

2.4.2. Investigation of DNA length on MH-Mg^{2+}-DNA complex.

To evaluate the capability of DNA binding with MH molecules, we evaluated the formation of DNA-Mg^{2+}-MH complex depending on the length of ssDNA. As shown in **Figure 14**, the encapsulation efficiencies for both MH and DNA increased rapidly with increasing Mg^{2+} concentration, after which further increasing Mg^{2+} concentration to 8 or 16 mM only slightly increased the encapsulation efficiencies of MH and DNA or even decreased. That means at 4 mM the encapsulation efficiencies of both MH and DNA reached saturation level, which is the ideal concentration for encapsulation efficiency.

Thus, further increasing on Mg^{2+} concentration had little effect on the loading efficiencies of MH and DNA. This result supports the hypothesis that the divalent metal ion (Mg^{2+}) plays an important role in the encapsulation yield of DNA and MH.

Furthermore, DNA length plays an important role in DNA and MH loading efficiency. As shown in **Figure 14 A & B**, when the length of DNA shorter than 15 nucleotides, the encapsulation yield of both MH and DNA are decreased even with optimized concentration (4mM of Mg^{2+}). In addition, the encapsulation capacity of different DNA lengths is affected by the molar ratio of MH to nucleotide. As shown in **Figure 14C**, at low Mg^{2+} concentrations (~ 1 mM), the molar ratio of MH/ nucleotide was >1. This ratio decreased to ~ 1 as increasing Mg2+ from 1 mM to 16 mM, which suggests that in the stable complex, MH binds to 1 nucleotide. However, polyA(11) shows abnormally high ratio of MH/nucleotide. This might be attributed to the errors at low entrapment yield.

The above results showed that the stable DNA-Mg^{2+}-MH particles could be formed with oligonucleotide > 11-nt through the electrostatic Mg^{2+} bridging interaction and pi-pi stacking between DNA nucleotide and MH. For short oligonucleotide, these molecular interactions are not strong enough (limit number of nucleotides) to hold ssDNA and MH together for particle formation, resulting in the low yield of DNA and MH encapsulation.

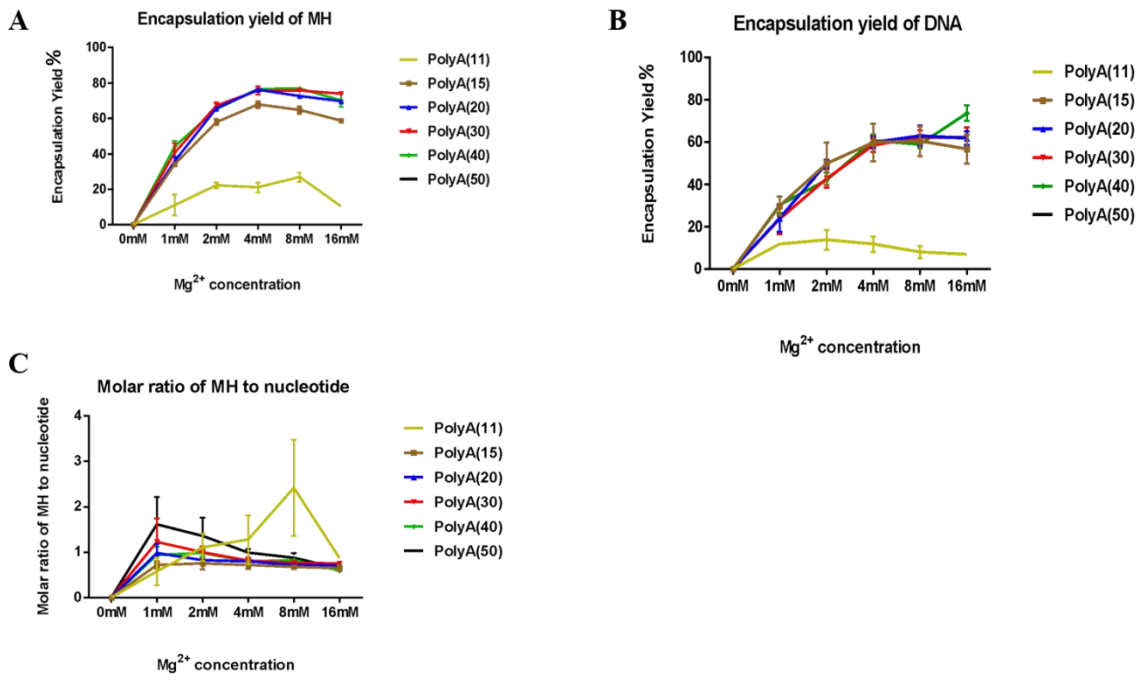

Figure 14. Loading yield of: (A) MH, (B) DNA, (C) molar ratio of MH to nucleotide with different lengths of DNA.

2.4.3. Investigation of different ssDNA bases for DNA-Mg^{2+}-MH complex.

Different types of nitrogen bases were evaluated for affecting the formation of DNA- Mg^{2+}-MH particles. As shown in **Figure 15**, four ssDNA strands of poly(A)20, poly(T)20, poly(C)20 and poly(G)20 were studied for forming DNA-MH particles in the presence of Mg^{2+}. All four-ssDNA encapsulated MH with similar yield, and reached maximal encapsulation yield at ~ 4 mM Mg^{2+} (**Figure 15 A**). However, in the DNA-Mg^{2+}-MH complex, poly(C)20 and poly(G)20 were more than poly(A)20 and poly(T)20 (**Figure 15B**). As a result**,** the molar ration of MH/ nucleotide was ~ 1 for poly(A)20 and poly(T)20, but this ratio dropped to ~ 0.5 for poly(C)20 and poly(G)20. Poly(C) and poly(G) encapsulated less MH than poly(A) and poly(T) in the formed particles. The possible reason is that C and G bases have secondary structure called C-rich DNA strands and G-

rich sequences (G- quadruplex), respectively. The self-folded poly(C) and poly(G) will push out MH from binding with nucleotides inside the structure, resulting in low entrapment efficiency of MH molecules.

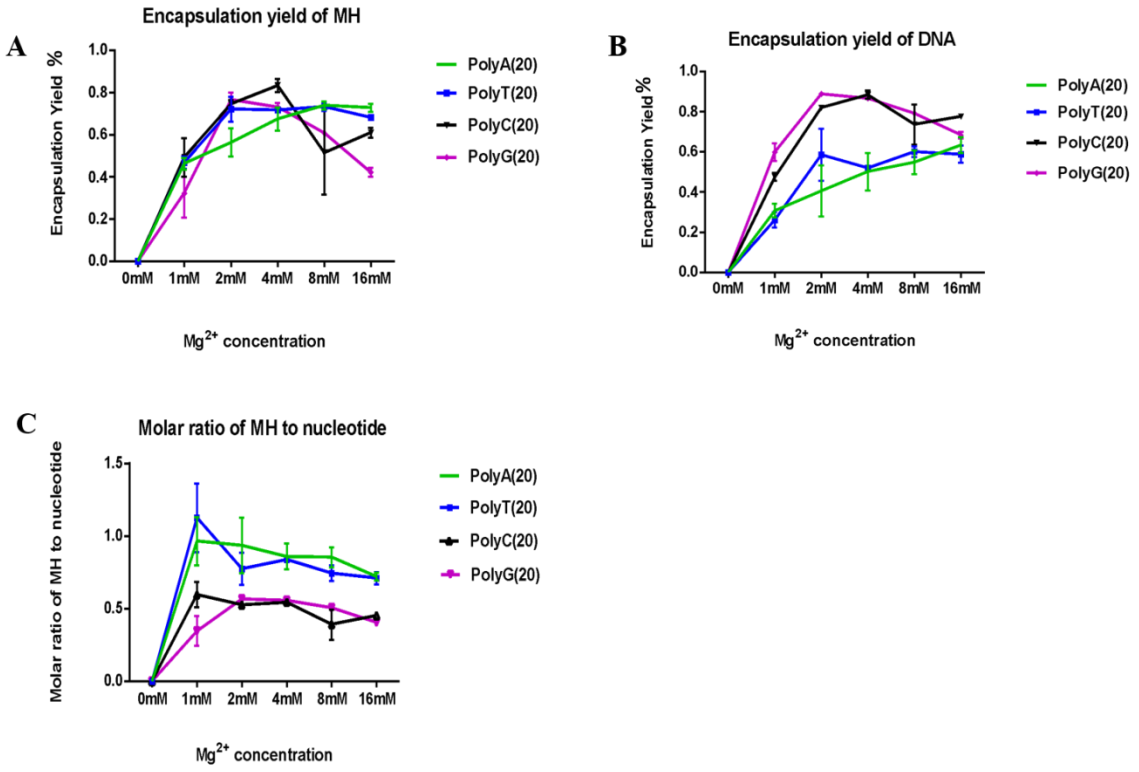

Figure 15. Loading yield of: (A) MH, (B) DNA, (C) molar ratio of MH to nucleotide with different nitrogen bases of ssDNA.

2.4.4. Compare ssDNA and dsDNA for DNA-Mg^{2+}-MH complex.

As shown in **Figure 16**, we compared single stranded DNA (ssDNA) and double-stranded DNA (dsDNA) for encapsulating MH under the presence of Mg^{2+}. Both ssDNA of poly(A)20 and Poly(C)20, and dsDNA of poly(AT)20 and poly(CG)20 reached the maximum encapsulation yield of MH at ~ 4 mM Mg^{2+}. However, in the DNA- Mg^{2+}-MH particles, the DNA precipitation ratio of poly(C)20 and poly(CG)20 (~ 0.8) were ~ 2-fold

more than the precipitation ratio of poly(A)20 and poly (AT)20 (~ 0.4) at 4 mM Mg^{2+}. Thus, the ratio of MH-to-nucleotide for poly(C)20 and poly(CG)20 was ~ half of the value for poly(A)20 and poly(AT)20. This result was consistent with the previous study that poly(C)20 and poly(G)20 were less efficient for entrapping MH than poly(A)20 and poly(T)20. They can range to each other forming a new structure that can conserve their structure from interaction with MH.

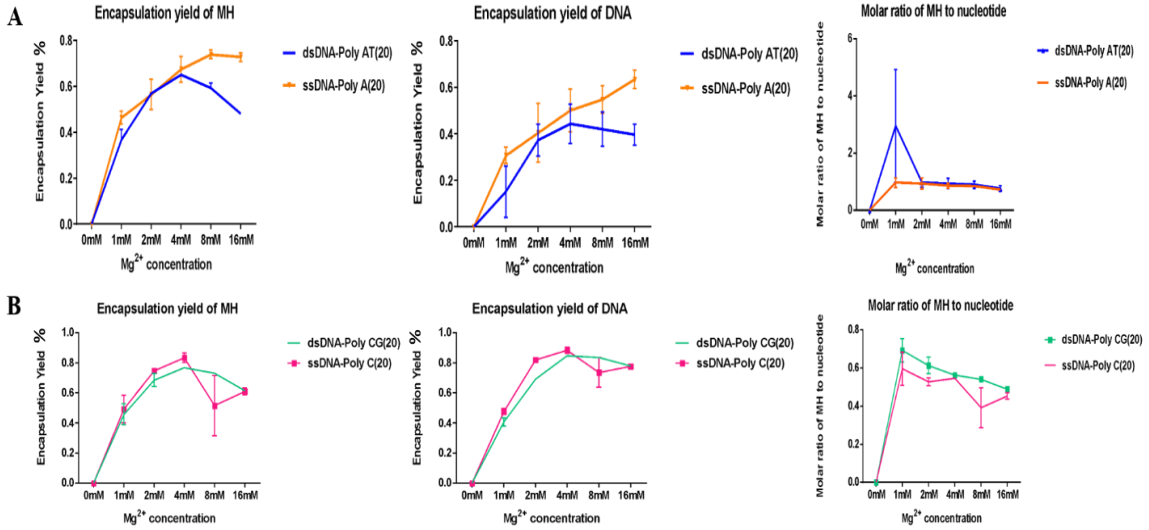

Figure 16. Loading capacity of ssDNA vs. dsDNA: (A) entrapment efficiency of MH, DNA, and MH/nucleotide for PolyAT-20 & PolyA-20 (B) entrapment efficiency of MH, DNA, and MH-to-nucleotide for PolyCG-20 & PolyC-20.

2.5. Conclusion.

In this chapter, we have investigated various conditions for the formation of DNA-Mg^{2+}-MH particles. First, Mg^{2+} played an important role as an electrostatic bridging agent to bring DNA and MH together, and stabilized the complex. By titrating Mg^{2+}

concentration, it was observed that the maximum yield of particle formation was reached at ~ 4 mM Mg^{2+}. Further increase of Mg^{2+} concentration could reduce the formation yield of particles formation due to the fact that high Mg^{2+} concentrations saturate each individual component of DNA and MH without the formation of bridged structure. Next, we tested the different lengths of poly-nucleotide for forming DNA- Mg^{2+}-MH particles, and it was found that a minimum length of 15-nt was required to form stable particles. The types of nitrogen bases also affected the yield of DNA- Mg^{2+}-MH complex. Poly(A) and poly(T) are more efficient to entrap MH than poly(C) and poly(G), possibly due to the fact that poly(C) and poly(G) tends to self-folded into secondary tetraplexes structures via hydrogen bonding between bases. The folded structures pushed out MH from binding to internal nucleotides, and resulted in lower entrapment efficiency of MH molecules. In addition, both ssDNA and dsDNA could form particles with MH, and the entrapment efficiency was dependent on the nitrogen bases.

Chapter 3

Structural Characterization of DNA-Mg^{2+}-MH complex And Control of Release of MH molecules

Abstract

In this chapter, we used multiple techniques to characterize the DNA-Mg2+-MH complex. Atomic force microscope (AFM) was used to visualize the nanostructure of particles, as well as the time-dependent formation kinetics, attenuated total reflectance (ATR-FTIR) is used to characterize the vibrational absorbance of key functional groups and water content. We also performed some preliminary study of MH release from DNA-Mg^{2+}-MH particles.

3.1. Materials and methods.

3.1.1. Materials for studying AFM and ATR-FTIR.

Highest Grade V1 Mica Disc, 12 mm was purchased from TED PELLA, INC. Tris base and acetic acid buffer (10 × TA) were purchased from Fisher Scientific (Waltham, MA.) and Mallinckrodt, respectively. DNA grade water and Magnesium acetate tetrahydrate (MgAc) were purchased from Fisher Scientific (Waltham, MA.). DNA bases were purchased from Integrated DNA Technologies (IDT). Minocycline hydrochloride was purchased from Sigma (St. Louis, MO.).

3.1.2. Preparation of MH-Mg^{2+}-DNA complex for AFM.

DNA oligonucleotides was dissolved in DNA grade water. The solution's concentration was measured by Nanodrop 2000 (Thermo Scientific). Minocycline solution

was prepared in DNA grade water. DNA-MH solution was mixed with equal mass concentration (1mg/ml) followed by the addition of magnesium acetate (4mM), 1 X TA buffer (PH 7.0), and deionized water (DI). The complex solution was diluted to 2 Fold dilution with (1 X TA Mg^{2+} 4mM, PH=7). Then, 2uL of the solution was dropped onto the center of a freshly cleaved mica surface, followed by 80uL 1 X TA (PH 7.0) buffer on mica surface, and 2uL of 100mM Ni^{2+} to enhance the DNA adsorption. After two minutes, the solution was removed from the edge by using a Kim-wipe. Then, 80uL DiH2O was added and removed by a Kim-wipe. This process was repeated three times to wash off the salt from the mica surface. Then, it was dried for AFM imaging.

3.1.3 Preparation of MH-Mg^{2+}-DNA complex for ATR-FTIR.

PolyA(20) was dissolved in DNA grade water. The solution's concentration was measured by Nanodrop 2000 (Thermo Scientific). Minocycline solution was prepared in DNA grade water. DNA-MH solution was mixed with equal mass concentration (1mg/ml) followed by the addition of magnesium acetate (4mM), 1 X TA buffer (PH 7.0), and deionized water (DI). Then, 20uL of the solution was dropped onto the center of a mica surface. Then, it was dried for ATR spectra and flipped on the other surface. Also, PolyA(20)'s spectra was measured the same way as the complex and MH.

3.2. Results and discussion.

3.2.1. AFM Characterization.

As shown in **Figure 17 A & B,** an atomic force microscope image showed the nanostructures of DNA-Mg^{2+}-MH with the size distribution of ~ 100- 200 nm in length. These nanoparticles were composed of tight DNA- Mg^{2+}-MH complexes that were resistance to the rinse of water. Ting Zhang from the Fu lab performed a dynamic AFM

study of DNA Origami- Mg^{2+}-MH nanoparticles depending on Mg^{2+} concentrations, as shown in **Figure 18**. The dynamic AFM scanning showed that the nucleation of MH particles increased as the addition of more Mg^{2+}.

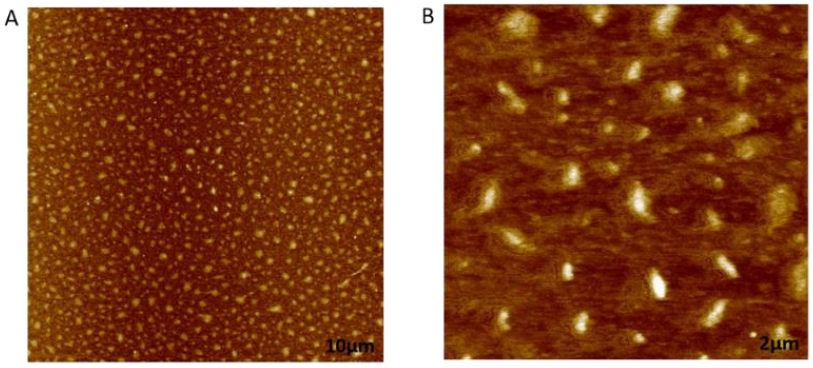

Figure 17. AFM imaging for PolyA (20)-Mg^{2+}-MH complex at (A) 10 μm scale and (B) 2 μm scale.

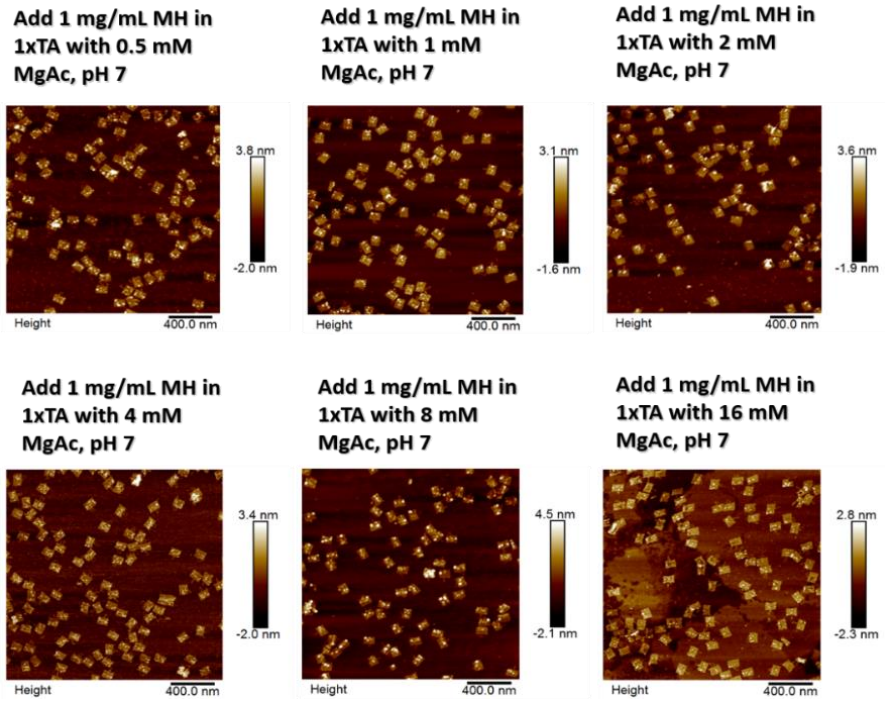

Figure 18. AFM imaging for Origami-Mg^{2+}-MH complex under different Mg^{2+} concentrations. Scale: 400 nm. Images are provided by Ting Zhang.

3.2.2. ATR-FTIR Characterization.

FTIR spectra in **Figure 19A** shows that MH peaked at ~1580 cm^{-1}, corresponding to C=O stretching on C10, which is part of a chelating site (C10-C11-C12) for Mg^{2+} ions. When the complex was formed with DNA and metal ions, this peak shifted to ~1600 cm^{-1} in the Mg^{2+}-based complex. **Figure 19B** illustrates that DNA(polyA-20) had an absorption peak of ~1210 cm^{-1}, which is phosphate group P=O**,** which shifted to ~1100 cm^{-1} in the Mg^{2+}-based complex (**Figure 19C).** IR spectrum also suggested that DNA- Mg^{2+}-MH complex may contain high content of water molecules, which resulted in the increased absorbance at 3,000 cm^{-1} to 3,500 cm^{-1}. However, IR study is preliminary, and comprehensive studies are required to better interpret the chemical groups and interactions in the complexes.

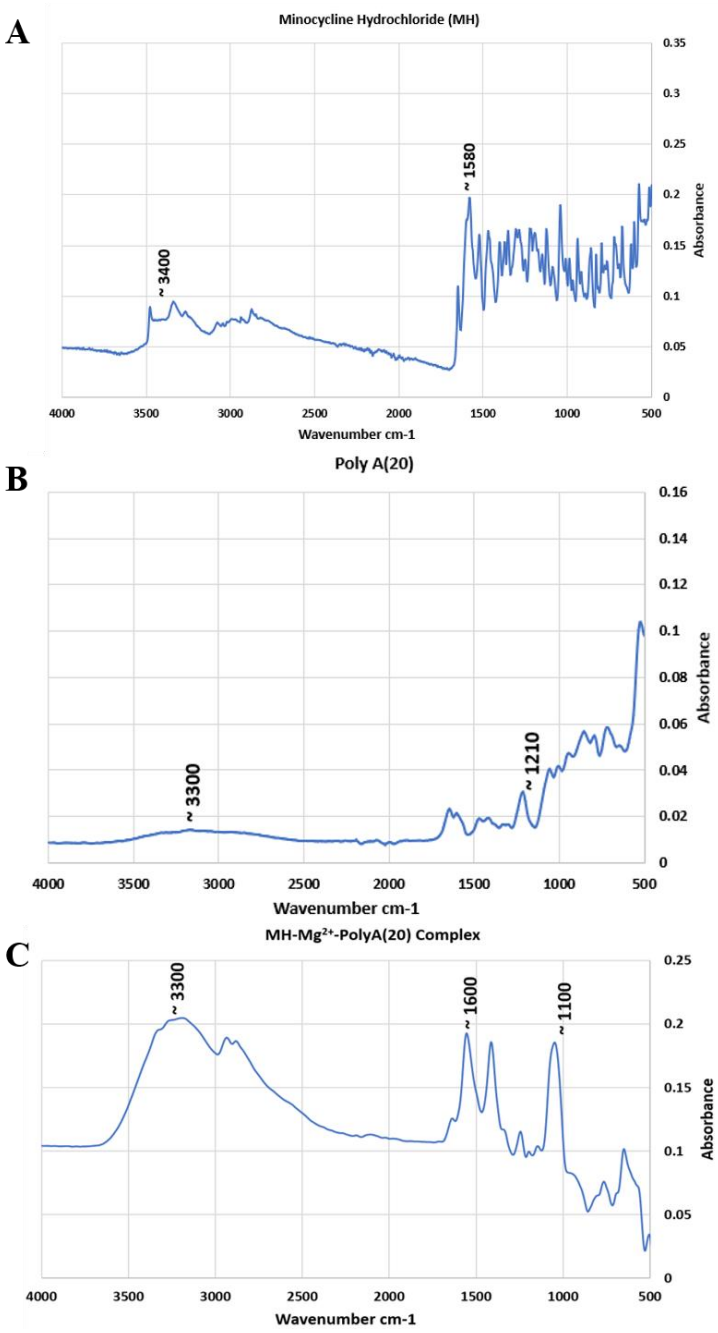

Figure 19. (A) FTIR spectrum for minocycline hydrochloride(MH), (B) FTIR spectrum for PolyA-20, (C) FTIR spectrum for PolyA(20)-Mg^{2+}-MH complex.

3.2.3. The release of MH molecules from DNA- Mg^{2+}-MH particles.

In collaboration with Dr. Ting Zhang from Fu lab and Ms Jia Nong from Prof.

Zhong lab at Drexel University, we characterized MH release kinetics from DNA-MH particles formed using different DNA nanostructures. The particles were prepared in agarose hydrogel. As shown in **Figure 20**, ssDNA of poly$(A)_{25}$ (poly-adenosine oligonucleotides) (blue) quickly released all MH within 6 days. Conversely, dsDNA of poly$(A\text{-}T)_{25}$ (green) had a much slower release rate (the release lasted for 20 days and is still going on). Crosslinked, multi-domain DNA hydrogel structure (red) released MH similarly as dsDNA-MH particles. The different releasing kinetics between ssDNA-MH and dsDNA-MH could be attributed to the strength of π-π stacking between them. ssDNA (purple) has flexible and dis-organized base groups with weaker π-π stacking between DNA bases and aromatic MH rings. Thus, ssDNA-MH complex is dominated by the electrostatic Mg^{2+} briding, which dissociates quickly in the physilogical buffer due to the ion competition from monovalent ions of Na^{+} and K^{+}. In contrast, π-π stacking between dsDNA and MH is more stable because the hydrogen-bonded base pairs are more geometrically organized and faciliated the π-π stacking and the subsequent intercalation of MH into dsDNA. Such phenomena have also been reported for other dsDNA-small molecule interactions, e.g. mythylene blue and doxorubicin. Thus, dsDNA-MH particles are much more stable than ssDNA-MH particles, which allows for extended duration of drug release. It is also noteworthy that a 2D DNA origami structure has a 9-day steady release rate as compared to the slow release from dsDNA and crosslinked DNA structures. Therefore, 2D DNA origami is highly promising to be used for high-dose release of MH for at least 7 days to target neuroprotection. Overall, these results show that we can design DNA nanostructures with different dimensions and folding layers to modulate the release of MH.

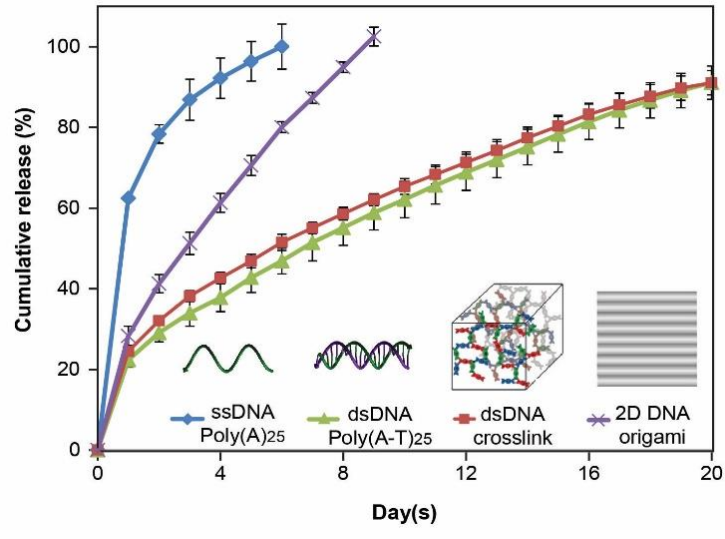

Figure 20. MH release kinetics from different DNA nanostructures: ssDNA (blue), dsDNA (green), crosslinked dsDNA hydrogel (red) and 2D DNA origami (purple). Images are provided by Ting Zhang.

3.3. Conclusion

We have used AFM and IR to characterize the DNA- Mg^{2+}-MH complex for learning more structural and chemical information. AFM results showed an average of 100 – 200 nm size for DNA- Mg^{2+}-MH nanoparticles which were stabilized by strong electrostatic ion bridging and pi-pi stacking between DNA bases and MH. A dynamic study also showed that smaller particles were first formed on the surface of DNA origami tiles at low Mg^{2+} concentration. As the addition of more Mg^{2+}, smaller nanoparticles started to crosslink each other and form large particle complexes. Preliminary IR study suggested a high content of water carried by the DNA- Mg^{2+}-MH complex. To explore the potential application, we tested the control of MH release using different DNA nanostructures-formed particles. This initial result could be potentially applied to controlling the release of MH in tissue therapy, such as spinal cord therapy.

Chapter 4

Conclusion and Future Perspective

In summary, we have studied the co-aggregation between DNA molecules and minocycline in the presence of magnesium (Mg^{2+}) which could be attributed to the effect of pi-pi stacking and the Mg^{2+} bridge between DNA phosphate and minocycline hydrochloride (MH).

We studied the DNA length for encapsulation efficiency of an insoluble complex, and it turns out that the efficiency of aggregate complex increased with DNA that shorter than 15 nucleotides. We also investigated whether there was any discrimination effect between DNA bases of A, T, C and G for binding to MH. It turns out that poly C and poly G have higher loading capacities for both MH and DNA than poly (A, T) as a result of the triple hydrogen bonding. Single-strand DNA (ssDNA) has a more effective reaction with MH than double-strand DNA (dsDNA) because of the rigid structure of dsDNA and the repulsive force between the phosphates in the dsDNA backbone. Where is the charge density of phosphates group on the surface of dsDNA be hindrance and decrease the interaction between dsDNA and MH.

For future plans, we will design multidimensional DNA nanostructures for controlling the release kinetics of MH. DNA nanostructures with multiple layers and dimensions will be used to adjust the surface-to-volume ratio and diffusion coefficient of drug-carrier nanoparticles that are critical for controlling drug release rate. To immobilize the particles at the injury site, the DNA-MH complexes will be prepared in agarose gel.

Toward this, we will investigating various DNA nanostructures for loading and releasing MH molecules to develop a robust drug delivery system with versatile release profiles. The outcome of the rearch will lay out the foundations for rational design of formulations capable of releasing MH with appropriate dose and duration: (1) high-dose MH release for at least 7 days to target neuroprotection; and (2) high dose of MH release for at least 7 days, followed by low-dose for at least 3 weeks to to target neuroprotection and chronic inflammation, respectively.

MH is a potential medicine for treating spinal cord therapy due to its anti-oxidant, anti-inflammatory, and anti-apoptotic properties.[24] [25]The MH-DNA complexes stabilized by magnesium ion (Mg^{2+}) could be loaded into agarose hydrogel for controlling MH release into medium. This might be useful in spinal cord therapy with continuous release of active MH in the tissue. The DNA-carried MH delivery system will be quite novel due to the capability of modulating the loading and release kinetics of drug molecules. As a carrier system, self-assembled DNA nanostructures have an inherent advantage of generating programmable nanostructures with controllable parameters of dimension, structural hierarchy and nanometer precision. As compared with conventional polymer-based drug delivery, the DNA-scaffold based drug delivery offers the advantages of 1) the ability to modulate multiple interactions between DNA and organic drug molecules including electrostatic metal ion bridging and pi-pi stacking; 2) the feasibility to easily tune the dimensional parameters of the molecular scaffold to carry drug molecules; 3) the control over the drug release kinetics by the rationally designed surface-to-volume ratio and drug diffusion through the multi-layer nanostructures; 4) the possibility of switching the release kinetics via the structural transformation of DNA nanostructures; 5) the ability

to offering an ideal drug release paradigm for spinal cord therapy. In addition to MH, DNA nanostructures can potentially be used to load and release proteins, peptides, and small molecule drugs such doxorubicin, daunorubicin and epirubicin. Therefore, this study not only leads to the development of an effective treatment for MH, but also has great potential to generate a variety of drug delivery systems for various biomedical applications in the future.

References

1. Fu, J.; Liu, M.; Liu, Y.; Yan, H., Spatially-interactive biomolecular networks organized by nucleic acid nanostructures. *Accounts of Chemical Research* **2012,** *45* (8), 1215-1226.

2. Seeman, N. C., DNA in a material world. *Nature* **2003,** *421* (6921), 427-431.

3. Bakewell, D. J.; Vergara-Irigaray, N.; Holmes, D., Dielectrophoresis of biomolecules. *JSM Nanotechnol Nanomed* **2013,** *1* (1), 1003-1027.

4. Pinheiro, A. V.; Han, D.; Shih, W. M.; Yan, H., Challenges and opportunities for structural DNA nanotechnology. *Nature Nanotechnology* **2011,** *6* (12), 763-772.

5. Linko, V.; Ora, A.; Kostiainen, M. A., DNA nanostructures as smart drug-delivery vehicles and molecular devices. *Trends in Biotechnology* **2015,** *33* (10), 586-594.

6. Fu, J.; Yang, Y. R.; Dhakal, S.; Zhao, Z.; Liu, M.; Zhang, T.; Walter, N. G.; Yan, H., Assembly of multienzyme complexes on DNA nanostructures. *Nature Protocols* **2016,** *11* (11), 2243-2273.

7. Ke, Y., Designer three-dimensional DNA architectures. *Current Opinion in Structural Biology* **2014,** *27*, 122-128.

8. Ke, Y.; Ong, L. L.; Shih, W. M.; Yin, P., Three-dimensional structures self-assembled from DNA bricks. *Science* **2012,** *338* (6111), 1177-1183.

9. Couvreur, P.; Vauthier, C., Nanotechnology: intelligent design to treat complex disease. *Pharmaceutical Research* **2006,** *23* (7), 1417-1450.

10. Kuzuya, A.; Komiyama, M., DNA origami: fold, stick, and beyond. *Nanoscale* **2010,** *2* (3), 309-321.

11. Lee, H.; Lytton-Jean, A. K.; Chen, Y.; Love, K. T.; Park, A. I.; Karagiannis, E. D.; Sehgal, A.; Querbes, W.; Zurenko, C. S.; Jayaraman, M., Molecularly self-assembled nucleic acid nanoparticles for targeted in vivo siRNA delivery. *Nature Nanotechnology* **2012,** *7* (6), 389-393.

12. Garrido-Mesa, N.; Zarzuelo, A.; Gálvez, J., Minocycline: far beyond an antibiotic. *British Journal of Pharmacology* **2013,** *169* (2), 337-352.

13. Wochner, A.; Menger, M.; Orgel, D.; Cech, B.; Rimmele, M.; Erdmann, V. A.; Glökler, J., A DNA aptamer with high affinity and specificity for therapeutic anthracyclines. *Analytical Biochemistry* **2008,** *373* (1), 34-42.

14. Zhu, G.; Zheng, J.; Song, E.; Donovan, M.; Zhang, K.; Liu, C.; Tan, W., Self-assembled, aptamer-tethered DNA nanotrains for targeted transport of molecular drugs in cancer theranostics. *Proceedings of the National Academy of Sciences* **2013,** *110* (20), 7998-8003.

15. Farokhzad, O. C.; Langer, R., Impact of nanotechnology on drug delivery. *ACS Nano* **2009,** *3* (1), 16-20.

16. Jewell, C. M.; Lynn, D. M., Surface-mediated delivery of DNA: cationic polymers take charge. *Current Opinion in Colloid & Interface Science* **2008,** *13* (6), 395-402.

17. Pack, D. W.; Hoffman, A. S.; Pun, S.; Stayton, P. S., Design and development of polymers for gene delivery. *Nature Reviews Drug Discovery* **2005,** *4* (7), 581-593.

18. Tang, M.; Szoka, F., The influence of polymer structure on the interactions of cationic polymers with DNA and morphology of the resulting complexes. *Gene Therapy* **1997,** *4* (8), 823-832.

19. Avakyan, N.; Greschner, A. A.; Aldaye, F.; Serpell, C. J.; Toader, V.; Petitjean, A.; Sleiman, H. F., Reprogramming the assembly of unmodified DNA with a small molecule. *Nature Chemistry* **2016,** *8* (4), 368-376.

20. Thorn, C. F.; Oshiro, C.; Marsh, S.; Hernandez-Boussard, T.; McLeod, H.; Klein, T. E.; Altman, R. B., Doxorubicin pathways: pharmacodynamics and adverse effects. *Pharmacogenetics and Genomics* **2011,** *21* (7), 440-446.

21. Alexander, C. M.; Maye, M. M.; Dabrowiak, J. C., DNA-capped nanoparticles designed for doxorubicin drug delivery. *Chemical Communications* **2011,** *47* (12), 3418-3420.

22. Jiang, Q.; Song, C.; Nangreave, J.; Liu, X.; Lin, L.; Qiu, D.; Wang, Z.-G.; Zou, G.; Liang, X.; Yan, H., DNA origami as a carrier for circumvention of drug resistance. *Journal of the American Chemical Society* **2012,** *134* (32), 13396-13403.

23. Zhao, Y.-X.; Shaw, A.; Zeng, X.; Benson, E.; Nyström, A. M.; Högberg, B. r., DNA origami delivery system for cancer therapy with tunable release properties. *ACS Nano* **2012,** *6* (10), 8684-8691.

24. Griffin, M. O.; Ceballos, G.; Villarreal, F. J., Tetracycline compounds with non-antimicrobial organ protective properties: possible mechanisms of action. *Pharmacological Research* **2011,** *63* (2), 102-107.

25. Pinney, S. P.; Chen, H. J.; Liang, D.; Wang, X.; Schwartz, A.; Rabbani, L. E., Minocycline inhibits smooth muscle cell proliferation, migration and neointima formation after arterial injury. *Journal of Cardiovascular Pharmacology* **2003,** *42* (4), 469-476.

26. Yrjänheikki, J.; Tikka, T.; Keinänen, R.; Goldsteins, G.; Chan, P. H.; Koistinaho, J., A tetracycline derivative, minocycline, reduces inflammation and protects against focal cerebral ischemia with a wide therapeutic window. *Proceedings of the National Academy of Sciences* **1999,** *96* (23), 13496-13500.

27. Humbert, P.; Treffel, P.; Chapuis, J.-F.; Buchet, S.; Derancourt, C.; Agache, P., The tetracyclines in dermatology. *Journal of the American Academy of Dermatology* **1991,** *25* (4), 691-697.

28. Giuliani, F.; Fu, S. A.; Metz, L. M.; Yong, V. W., Effective combination of minocycline and interferon-β in a model of multiple sclerosis. *Journal of Neuroimmunology* **2005,** *165* (1), 83-91.

29. Bonelli, R. M.; Heuberger, C.; Reisecker, F., Minocycline for Huntington's disease: an open label study. *Neurology* **2003,** *60* (5), 883-884.

30. Du, Y.; Ma, Z.; Lin, S.; Dodel, R. C.; Gao, F.; Bales, K. R.; Triarhou, L. C.; Chernet, E.; Perry, K. W.; Nelson, D. L., Minocycline prevents nigrostriatal dopaminergic neurodegeneration in the MPTP model of Parkinson's disease. *Proceedings of the National Academy of Sciences* **2001,** *98* (25), 14669-14674.

31. Xu, L.; Fagan, S. C.; Waller, J. L.; Edwards, D.; Borlongan, C. V.; Zheng, J.; Hill, W. D.; Feuerstein, G.; Hess, D. C., Low dose intravenous minocycline is neuroprotective after middle cerebral artery occlusion-reperfusion in rats. *BMC Neurology* **2004,** *4* (1), 7.

32. Bin, S.; Zhou, N.; Pan, J.; Pan, F.; Wu, X.-F.; Zhou, Z.-H., Nano-carrier mediated co-delivery of methyl prednisolone and minocycline for improved post-traumatic spinal cord injury conditions in rats. *Drug Development and Industrial Pharmacy* **2017,** *43* (6), 1033-1041.

33. Zhang, Z.; Wang, Z.; Nong, J.; Nix, C. A.; Ji, H.-F.; Zhong, Y., Metal ion-assisted self-assembly of complexes for controlled and sustained release of minocycline for biomedical applications. *Biofabrication* **2015,** *7* (1), 015006.

34. Sapadin, A. N.; Fleischmajer, R., Tetracyclines: nonantibiotic properties and their clinical implications. *Journal of the American Academy of Dermatology* **2006,** *54* (2), 258-265.

35. Nelson, M., Chemical and biological dynamics of tetracyclines. *Advances in Dental Research* **1998,** *12* (1), 5-11.

36. Good, M.; Hussey, D., Minocycline: stain devil. *British Journal of Dermatology* **2003,** *149* (2), 237-239.

37. Kim, H.-S.; Suh, Y.-H., Minocycline and neurodegenerative diseases. *Behavioural Brain Research* **2009,** *196* (2), 168-179.

38. Wang, Z.; Nong, J.; Shultz, R. B.; Zhang, Z.; Kim, T.; Tom, V. J.; Ponnappan, R. K.; Zhong, Y., Local delivery of minocycline from metal ion-assisted self-assembled complexes promotes neuroprotection and functional recovery after spinal cord injury. *Biomaterials* **2017,** *112*, 62-71.